Characterization of Pt Nanoparticles Deposited onto Carbon Nanotubes Grown on Carbon Paper and Evaluation of This Electrode for the Reduction of Oxygen

D. Villers, S. H. Sun, A. M. Serventi, and J. P. Dodelet*

INRS-Énergie, Matériaux et Télécommunications, 1650 Boulevard Lionel Boulet, Varennes, Québec, Canada, J3X 1S2

S. Désilets

R&D pour la Défense Valcartier, 2459 Boulevard Pie-XI Nord, Val-Bélair, Québec, Canada, G3J 1X5

Received: September 11, 2006; In Final Form: October 25, 2006

Multiwalled carbon nanotubes (MWCNTs) were grown on the fibers of a commercial porous carbon paper used as carbon-collecting electrodes in fuel cells. The tubes were then covered with Pt nanoparticles in order to test these gas diffusion electrodes (GDEs) for oxygen reduction in H_2SO_4 solution and in H_2/O_2 fuel cells. The Pt nanoparticles were characterized by cyclic voltammetry, transmission electron microscopy, and X-ray photoelectron spectroscopy. The majority of the Pt particles are 3 nm in size with a mean size of 4.1 nm. They have an electrochemically active surface area of 60 m^2/g Pt for Pt loadings of 0.1−0.45 mg Pt/cm^2. Although the electroactive Pt surface area is larger for commercial electrodes of similar loadings, Pt/MWCNT electrodes largely outperform the commercial electrode for the oxygen reduction reaction in GDE experiments using H_2SO_4 at pH 1. On the other hand, when the same electrodes are used as the cathode in a H_2/O_2 fuel cell, they perform only slightly better than the commercial electrodes in the potential range going from ∼0.9 to ∼0.7 V and have a lower performance at lower voltages.

Introduction

Polymer electrolyte membrane (PEM) fuel cells are electrical power generators based on two electrochemical reactions: the oxidation of hydrogen at the anode and the reduction of oxygen at the cathode. PEM fuel cells are presently drawing a great deal of attention because they are high efficiency, high energy density, and very low emission power generators.[1] Due to the very acidic pH of their membrane electrolyte, Pt is presently the only catalyst used in PEM fuel cell prototypes. Pt is an excellent catalyst to promote the anodic oxidation of hydrogen, but the story is not the same at the cathode where the oxygen reduction reaction (ORR) on Pt is rather sluggish in acidic medium. Consequently, Pt loadings at the cathode remain high, while low loadings may be used at the anode without compromising the fuel cell performance.[2]

Pt is a noble metal of limited supply. Presently, there are two main approaches in attempting to decrease the Pt loading at the cathode: the first one is alloying Pt with another (or several other) metal(s) in order to improve the ORR kinetics on the new catalysts;[3,4] the second approach is to use Pt nanoparticles on different catalyst supports since it is known that the support may significantly affect the catalyst performance.[5−8]

The usual supports for electrocatalysts are high surface area carbon blacks with high mesoporous content and a degree of graphitic character. Ideal supports for electrocatalysts should also have the following characteristics: provide a high electrical conductivity, allow good reactant gas access to the electrocatalyst, have adequate water handling capability (particularly at the cathode where water is generated in PEM fuel cells), and also show good corrosion resistance, especially under the highly oxidizing conditions which occur at the cathode.[3] Some carbon blacks like Vulcan XC-72R, for instance, display all the above-mentioned characteristics. However, it is possible that a fraction of Pt nanoparticles dispersed on these carbon blacks is trapped in the pores of the carbon electrode, where the three-phase boundary between gas, electrolyte, and electrode cannot be established. Therefore, it is possible that other carbon species like carbon nanotubes, which have rather large surface areas but little porosity, may be better supports for Pt nanoparticles. Indeed, besides being practically devoid of microporosity (except for the hollow interior of the tube, which is not always open), multiwalled carbon nanotubes (MWCNTs) are also good electrical conductors,[9] have a high tensile strength,[10] display an excellent resistance to electrochemical corrosion,[11,12] and are expected to have a high gas permeability, especially if they are oriented.[13]

A large body of studies related to the use of carbon nanotubes as supports for Pt nanoparticles appeared recently in the literature. These studies have been reviewed by Lee et al.,[14] who also reported on carbon nanofibers for the same use. Typically, this literature[15−38] describes a procedure to obtain Pt particles on carbon nanotubes that are then characterized physically (SEM, TEM, XRD, XPS, etc.). Most of the studies complete this physical characterization by describing the electrochemical behavior of these electrodes in cyclic voltammetry either for the oxidation of methanol or (and) for the reduction of oxygen. Only a few studies report the fuel cell behavior of Pt/carbon nanotube at the cathode of H_2/O_2 fuel cells or direct methanol fuel cells.[11,13,39−52] The electrochemical performance of Pt/carbon nanotube is sometimes compared with that reported for Pt/carbon black. When this is done for cyclic

* Corresponding author. E-mail: dodelet@emt.inrs.ca.

10.1021/jp065923g CCC: $33.50
Published on Web 12/07/2006

voltammetry studies, the performance of Pt/carbon nanotube is always better than that for Pt/carbon black.[22,28,29,31,32,34] For fuel cell measurements, however, the results are not consistent. Some studies report better performance for Pt/carbon nanotubes,[13,40,41,45,48,50,52] while others report equivalent or better performance for Pt/carbon black.[42,44,47−49]

Practically all reported studies were conducted with Pt nanoparticles on loose carbon nanotubes. As Pt does not wet the carbon nanotubes,[53] anchoring points are usually obtained by oxidizing the nanotube first with a strong chemical oxidant like HNO_3, a mixture of H_2SO_4 and HNO_3, $K_2Cr_2O_7$, $KMnO_4$, or H_2O_2.[51,54−56] As a result of this treatment, hydroxyl, carbonyl, and carboxyl functionalities appear on the nanotubes and help to interact with Pt precursors and ultimately with Pt nanoparticles. The oxidation step may also be performed electrochemically.[16,20] Various Pt precursors and reduction procedures were used to obtain Pt nanoparticles/carbon nanotubes. By far, the most common one was the reduction of H_2PtCl_6 (or K_2PtCl_6) in alcohol or poly alcohol (like ethylene glycol), usually in basic pH, with or without the addition of another reducing agent like $Na_2S_2O_4$, $NaBH_4$, or formaldehyde.[13,15,17,19,22−24,29,33,34,38,41,42,46,47,49,51] Carbon nanotubes were also functionalized with special functionalities like SH, NH_2, SO_3H, and COOH[11,21,26,31,37,50,52] to interact with the Pt precursor or even with colloidal Pt as in the case of SH. Besides the simple adsorption of Pt black onto carbon nanotubes,[32] dc sputtering of Pt,[25] electrochemical reduction of H_2PtCl_6 (or Na_2PtCl_6),[16,28,35,44] and electroless deposition[30,36,39] were also used to obtain Pt nanoparticles/carbon nanotubes. Except for the electrochemical and electroless methods for which Pt particles were usually rather large,[16,30,35,36,44] the Pt nanoparticles obtained were always small (usually less than 5 nm on average). The largest Pt loadings on carbon nanotubes were obtained by simple adsorption of Pt black (40 wt %),[32] thiolation of the nanotube (40 wt %),[31] and reduction of ethylene glycol (30 and 28 wt %).[13,47]

As carbon paper is used in fuel cells as charge-collecting electrodes, we proposed, a while ago, to grow MWCNTs on carbon paper, and then load the nanotubes with Pt nanoparticles to obtain a PEM fuel cell cathode. Preliminary results were presented in ref 57. The idea of growing carbon nanotubes on carbon paper was also exploited by Yan and co-workers[44,48,50] who showed that interesting polarization curves could be obtained with such cathodes. Contrary to Yan and co-workers who use either electrochemical deposition of Pt on the nanotubes, spray a Pt precursor (H_2PtCl_6) before reducing it in hydrogen, or functionalize the nanotubes with a diazonium salt to anchor H_2PtCl_6, which is then reduced to obtain Pt nanoparticles, we use a silane derivative to obtain SO_3H functionalities on the nanotube without oxidizing it first. This procedure enables the exchange of Pt^{4+} cations for protons. Platinum nanoparticles are obtained on the nanotube by a subsequent reduction of the Pt precursor. The same silane derivative is also used for the deposition on the carbon paper of Co−Ni catalytic particles that are used to grow the nanotubes. This paper presents the optimization of the Pt loading on carbon nanotubes and the use of these electrodes as cathodes in gas diffusion electrodes (GDEs) for the reduction of oxygen in H_2SO_4 solutions and H_2/O_2 fuel cells.

Experimental Section

Preparation of MWCNTs on Carbon Paper and Pt Deposition on the Nanotubes. Multiwalled carbon nanotubes were grown on carbon fuel cell backing paper (0.17 mm thick, 81% porosity) purchased from E-TEK, Division of DeNora. The carbon fibers of the paper were seeded with Co−Ni catalytic particles obtained by dipping the paper in a mixture of ethanol (93% in volume), water (6%), and silane (1%) containing 0.3 M $Ni(NO_3)_2$ and 0.3 M $Co(NO_3)_2$ (0.6 M Co−Ni salts, combined). Here silane is 2(4-chlorosulfophenyl) ethyltrichlorosilane, 50 vol % in dichloromethane from Gelest Inc., Morrisville, PA. The carbon paper was soaked for 2 h in the silane solution before being removed and dried in air.

The growth of MWCNTs was performed in a specifically designed CVD reactor taking advantage of the fact that the carbon paper was the most resistive part of an electrical circuit and could therefore be heated by Joule effect. Once the carbon paper loaded with catalyst was fixed into the CVD reactor, it was purged with Ar (550 standard cubic centimeters per min; sccm) for 20 min. Then the Ar flow was decreased and H_2 was added (350 sccm for Ar and 1.5 sccm for H_2). After 2 min of such reducing gas flow, the temperature was raised to about 600 °C for 2 min, to obtain Co−Ni nanoparticles, and then it was increased to 800 °C before introducing ethylene (C_2H_4; 16 sccm) which serves as carbon feedstock to grow the nanotubes. The temperature was maintained at 800 °C for 6 min. Then the H_2 and C_2H_4 flows were stopped and the Ar flow was increased to 550 sccm before turning the heating system off and letting the temperature decrease to room temperature. More details on the MWCNT growth procedure can be found elsewhere.[58,59] The experimental conditions for Pt deposition onto the MWCNTs will be optimized in the Results and Discussion.

Characterization of the Electrodes. *Microscopy.* A Hitachi S-4700 field emission scanning electron microscope (FE-SEM) operated at 5 kV was employed to characterize the morphology of the MWCNTs. The nanostructural investigation of the samples was carried out by using a Hitachi H-9000NAR high-resolution transmission electron microscope (HRTEM) operated at an accelerating voltage of 300 kV. Conventional and high-resolution TEM imaging of the samples and selected area electron diffraction (SAED) were carried out to understand their structure and composition. Samples for TEM investigation were directly cut from the carbon paper.

Elemental Analysis. Surface elemental analysis was performed by X-ray photoelectron spectroscopy (XPS) using a VG Escalab 200i instrument. The Al Kα line (1486.6 eV) was chosen as the X-ray source. The pass energy was 20 eV, and the energy increment was 0.1 eV. Narrow scan photoelectron spectra were recorded for Pt. The quantification of the detected elements and the spectra deconvolution were performed using Casa XPS software. For Pt in its metallic state, a Gaussian/Lorentzian line shape modified by an asymmetric function was used to reflect the asymmetric tail of the peaks toward higher binding energies[60]

Bulk elemental analysis was performed by neutron activation analysis of the samples at École Polytechnique de Montréal.

Specific Area of the Electrode. The specific area of the electrode was determined by BET analysis, using an Autosorb-1MP instrument and ASI Win software from Quantachrome.

Electrochemical Characterization. Three types of electrochemical characterization were performed.

The first one consisted in determining the active Pt area. It was obtained by cyclic voltammetry (Figure 1), in a three-electrode/one-compartment cell containing deaerated H_2SO_4 at pH 1, using a PAR 273A potentiostat controlled by Corrware software. The working electrode was a piece of carbon paper 0.4 cm wide by 1.5 cm long covered at only one extremity with MWCNTs on which Pt nanoparticles were deposited according to the silane procedure. The coverage area was approximately

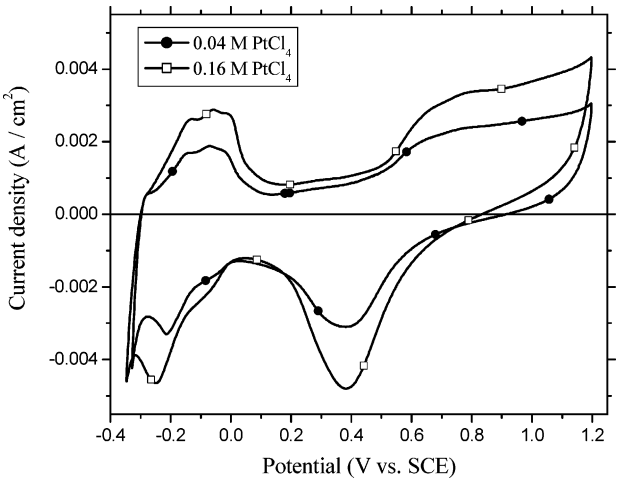

Figure 1. Cyclic voltammetry, at 10 mV/s, in a deaerated solution of H_2SO_4 at pH 1 of Pt−MWCNTs−fuel cell backing electrodes from two solutions, 0.04 and 0.16 M, of $PtCl_4$ in 93% ethanol + 6% water + 1% silane.

0.4 cm × 0.4 cm. The uncovered remainder of the carbon paper was mated with a Cu support and held firmly together using Parafilm to ensure electrical contact. The active surface of the electrode was therefore 0.16 cm^2 × 2 = 0.32 cm^2, since the carbon paper with nanotubes was active on both sides. Before dipping the electrode in the electrolyte, the part to be analyzed was dipped in acetone in order to increase the wettability of the nanotubes in aqueous solution. Then it was rinsed with deionized water. The reference electrode was saturated calomel (SCE). The counter electrode was a Pt foil. Before running any experiment, the solution was thoroughly deaerated by bubbling N_2 during 30 min, and a N_2 atmosphere was kept over the solution during voltammetry. The Pt-on-nanotube electrode was also activated by cycling between about −0.3 to about 1.2 V vs SCE (avoiding H_2 or O_2 evolution) until the last cycle was superposable on the previous one. The voltammetry scan rate was 10 mV/s. The charges corresponding to the electroactive surface of Pt were measured under the electroadsorption curve of hydrogen, usually between about 0 to about −0.3 V, on the negative scan of the potential (see Figure 1). Commercially available Pt-catalyzed ELAT carbon cloth from E-TEK was used for comparison. The Pt loading of these commercial electrodes was either 10 or 20 wt % Pt/C, corresponding to a Pt density of 0.35 or 0.40 mg Pt/cm^2, respectively. The charges measured under the electroadsorption curves for hydrogen with the two commercial electrodes were Q_H = 70 and 82 mC/cm^2, respectively. The Pt area was determined electrochemically according to the following formula:

$$S_{EL} = Q_H/(Q_{ref}(\text{Pt loading}))$$

S_{EL} is expressed in cm^2/mg Pt, where Pt loading is in mg Pt/cm^2 and Q_{ref} = 0.21 mC/cm^2. This value corresponds to a surface density of 1.3 × 10^{15} atoms of Pt per cm^2, a generally accepted value for a polycrystalline Pt electrode.[61]

$$S_{EL} \text{ in } m^2/\text{g Pt} = 0.1 S_{EL} \text{ in } cm^2/\text{mg Pt}$$

When the average size of Pt particles is known, it is also possible to calculate the actual Pt surface area, S_{actual}, according to the following formula:

$$S_{actual} = 60\,000/(\rho d)$$

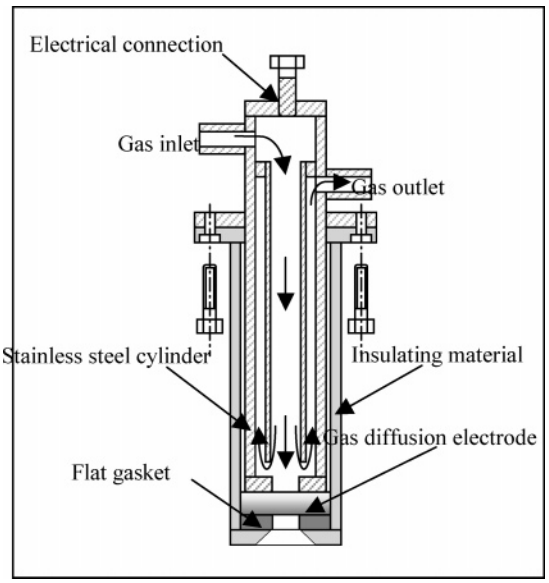

Figure 2. GDE setup used to characterize the Pt−MWCNTs−fuel cell backing electrodes for the electroreduction of oxygen in H_2SO_4 at pH 1.

S_{actual} is expressed in cm^2/mg Pt when ρ, the Pt density, is given in g/cm^3 and d, the average diameter of the Pt particles, is given in nm. If the distribution of Pt particles is known,

$$S_{actual} = 0.01\Sigma(60\,000 N_i)/(\rho d_i)$$

where N_i is the percentage of particles having a size d_i.

$$S_{actual} \text{ in } m^2/\text{g Pt} = 0.1 S_{actual} \text{ in } cm^2/\text{mg Pt}$$

The second electrochemical characterization consisted in the evaluation of the Pt-loaded MWCNT electrode in a GDE setup. The GDE experiments were conducted with the GDE setup described in Figure 2, using a PAR 273A potentiostat controlled by Corrware software. The GDE is used as the working electrode in a two-compartment cell, the Pt counter electrode being separated from the main compartment by a Nafion 117 membrane. The reference electrode was again a saturated calomel electrode. Before being inserted in the GDE setup, the disk (0.97 cm diameter, 0.74 cm^2) of Pt-loaded MWCNTs grown on carbon backing was first covered with 20 μL of a Nafion recast solution (5 wt % Nafion in alcohols/water mix, from Aldrich) and vacuum-dried at 75 °C for 1 h. The dimension of the electrode in contact with the solution was a circle of 0.44 cm diameter (0.15 cm^2). The H_2SO_4 solution at pH 1 in contact with the nanotubes was deaerated by bubbling nitrogen for 20 min before starting the experiment. A N_2 flow was also maintained during the experiment. Oxygen was introduced at different flows in the GDE (between 8 and 154 cm^3/min). However, changing the oxygen flow in the GDE had very little effect on the GDE results. All polarization curves were produced at a scan rate of 0.5 mV/s between 0.8 and −0.3 V vs SCE. The cell resistance was measured by impedance spectroscopy. Typically, the cell resistance was 0.9 Ω cm^2 for ELAT; for GDEs made of Pt/MWCNTs, the cell resistance was 1.2 Ω cm^2 when Pt was deposited (1−3 depositions) from a 0.04 M Pt halide solution and 0.6 Ω cm^2 when Pt was deposited (one deposition step) from a 0.16 M Pt halide solution.

The third electrochemical characterization consisted in evaluating the Pt-loaded MWCNT electrode as the cathode in H_2/O_2 fuel cell tests. These tests were performed in a Globe Tech GT60

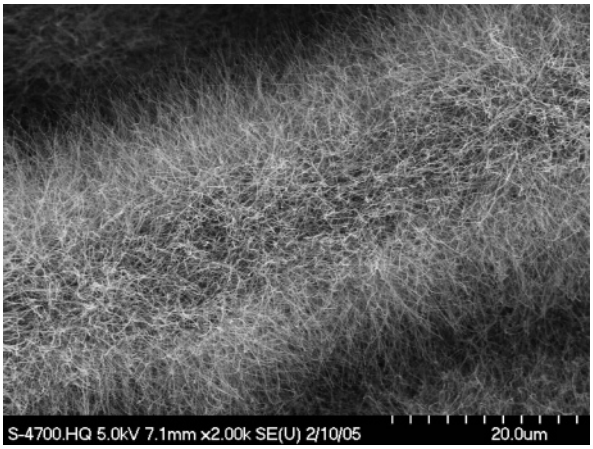

Figure 3. SEM micrograph of carbon nanotubes obtained after 6 min of synthesis with Co−Ni catalysts from a 93% ethanol + 6% water + 1% silane solution of 0.6 M Co−Ni salts. The carbon feedstock is C_2H_4, and the synthesis temperature is 800 °C.

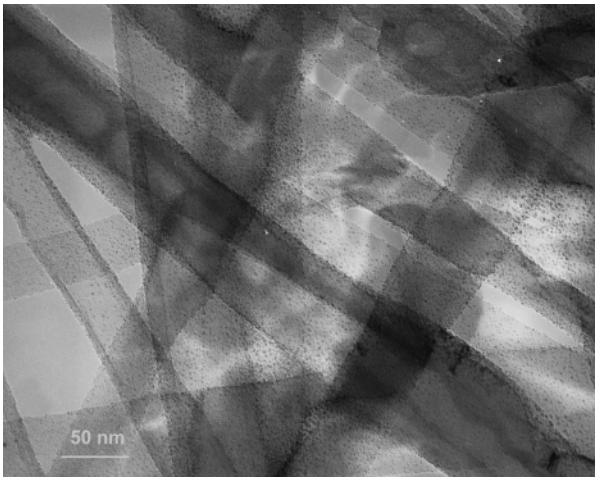

Figure 4. TEM micrograph of MWCNTs homogeneously covered with the precursor of the Pt particles from a 0.04 M $PtBr_4$ solution in 93% ethanol, 6% water, and 1% silane.

fuel cell test station. The membrane electrode assembly was prepared according to the following procedure: An ELAT 10% Pt/C, with a loading of 0.35 mg Pt/cm^2, was used as the anode, while the cathode was carbon paper backing with Pt on carbon nanotubes. The membrane was Nafion 117. The electrode area was 1.09 cm^2 on which 62 μL of a Nafion recast solution (Aldrich) was cast. The electrodes were dried under vacuum at 75 °C for 3 h. The carbon nanotube electrode backings were hydrophobically treated by spraying them with <1 mg/cm^2 PTFE/Vulcan XC-72 mixture (1:3 weight ratio in 2-propanol). The MEA was heat-pressed at 140 °C, first at 500 lb (pounds) for 1 min, then at 950 lb for 40 s. The MEA was then loaded in the fuel cell test hardware for polarization curve measurements. Fuel cell conditions were as follows: P_{H2} = 30 psi (pounds per square inch), P_{O2} = 60 psi, H_2 flux = 0.5 slm (standard Liter per min), O_2 flux = 0.5 slm. Humidifier temperature = 110 °C for H_2 and 90 °C for O_2. The MEA was conditioned for 4 h at a constant potential (0.5 V vs DHE (dynamic hydrogen electrode)). The cell resistance was measured by impedance spectroscopy. This was followed by measurements of the polarization curve. Typically, the cell resistance was between 0.14 and 0.16 Ω cm^2.

Results and Discussion

Deposition and Characterization of Pt Nanoparticles onto MWCNTs. The morphology of MWCNTs grown on the carbon fibers of a fuel cell backing is shown in Figure 3. Here the carbon nanotubes were grown for 6 min at 800 °C by the decomposition of ethylene on the Co−Ni catalytic nanoparticles deposited onto the fibers of the carbon paper. The SEM micrograph reveals a high density of nanotubes uniformly grown on the whole surface of the fiber. A micrograph at lower magnification, depicting MWCNTs covering several fibers, is shown in the Supporting Information (Figure S1). The tubes are tip grown. They are generally straight and are about 12 μm long. TEM pictures appearing in the following figures indicate that these nanotubes have diameters ranging from 40 to 70 nm. The typical specific area of the carbon paper alone is approximately 1 m^2/g. This area is increased to 60 m^2/g when the carbon paper is covered with carbon nanotubes.

Platinum deposition was carried out on the nanotubes using the same silane derivative as that used to obtain Co−Ni catalyst particles, but this time, using a Pt precursor instead of a Co−Ni precursor. MWCNTs were immersed in a 1% silane solution in 93% ethanol and 6% H_2O containing 0.04 M $PtCl_4$ or 0.04 M $PtBr_4$. After 2 h of immersion, they were removed from the solution and let to dry in air. It is expected that, besides being deposited onto the nanotubes, Pt particles are also deposited onto the carbon fibers which support the carbon nanotubes. However, on the basis of their respective surface area, the amount of Pt particles deposited onto the carbon fiber is expected to be at least 60 times lower than the amount of Pt particles deposited onto the nanotubes.

Analysis of the depositions obtained before performing any reduction of the Pt precursor reveals interesting results. Figure 4 shows the distribution of the Pt precursor on the carbon nanotubes. It shows that numerous small particles of Pt precursor of about 3 nm in size are homogeneously distributed over the entire surface of the nanotubes. A Pt4f narrow scan XPS spectrum of the Pt precursor distributed over the MWCNTs is presented in Figure 5A. The deconvolution of the XPS spectrum shows that even before the reduction of the Pt precursor, Pt(0) is already detected and represents about 31% of all Pt found in the precursor. Oxidized Pt is mainly found as Pt(II), which represents 68%, while the presence of Pt(IV) is marginal at about 1%, even though only Pt(IV) was used in the silane solution. However, an electrochemical determination of the active Pt surface indicates a very small Q_H charge (less than 5 mC/cm^2). So, even if metallic Pt is present on the electrode, it is probably mixed with an insulating material (it will be identified later as $PtCl_2$) and has poor electrical contact with the nanotube.

We do not know exactly why some spontaneous Pt reduction of the precursor occurs on these electrodes. The first possible explanation that comes to mind is that ethanol is a reductant and reduces Pt salts to metallic Pt. However, this is highly improbable since Pt solutions in 93% ethanol, 6% H_2O, and 1% silane remain clear at room temperature for several months, unlike solutions using ethylene glycol that become black within a week. An alternative explanation may be found in a recent report from Qu and Dai[30] where they showed that metals like Pt, Au, and Pd may be deposited electrolessly on carbon nanotube if those are in electrical contact with a metallic substrate like Cu. Here, the Co−Ni catalyst that was used to grow the nanotubes is still present at the tip of each MWCNT. It should, however, not be in contact with the electrolyte, but it is possible that some of the several thousands of nanotubes that cover every carbon fiber may be broken and would open a channel for the electrolytic solution to the Co−Ni metal, the latter playing a similar role to Cu in Qu and Dai's report. Any

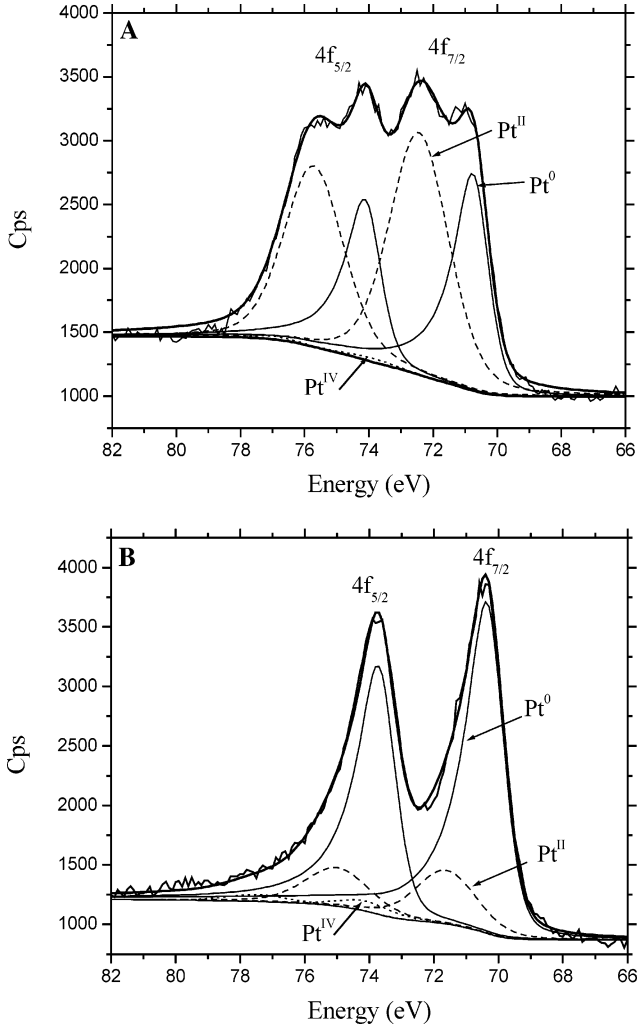

Figure 5. (A) Pt4f XPS narrow scan spectrum of the Pt particle precursor deposited from a 0.04 M $PtBr_4$ solution using the silane procedure. (B) Pt4f XPS narrow scan spectrum of the Pt particles obtained after chemical reduction (H_2/Ar) at 500 °C of the Pt precursor deposited from a 0.04 M $PtBr_4$ solution using the silane procedure.

other metallic impurity in the silane solution with a formal potential more negative than Pt(IV)/Pt(0) will also reduce Pt(IV) in the precursor.

The MWCNTs with the Pt precursor were then chemically reduced for 15 min in an oven at various temperatures ranging from 100 to 900 °C in a flow of H_2 and Ar (3:1; in volume). Figure 6 shows the evolution of the electrochemically active surface (expressed in terms of Q_H) of these electrodes with the reduction temperature. Although Figure 6 shows some scattering mainly due to differences in the density of MWCNTs on the electrodes, it is clear that Q_H increases with the reduction temperature for both $PtBr_4$ and $PtCl_4$ precursors and that it tends to stabilize around 25 mC/cm^2 for reduction temperatures of 500 °C and above. A typical TEM micrograph and its corresponding histogram showing the distribution of Pt particles on the MWCNTs after reduction at 500 °C are shown in Figure 7, parts A and 7, respectively. Most of the Pt particles have a size ranging from 2 to 7 nm with a most probable occurrence at 3 nm and an average size of 4.1 nm. Similar TEM results were obtained for both $PtBr_4$ and $PtCl_4$ precursors. As expected, larger particles also became more numerous as the reduction temperature increased (not shown).

The Pt4f narrow scan XPS spectrum of a MWCNT electrode loaded with Pt precursor reduced at 500 °C is presented in Figure

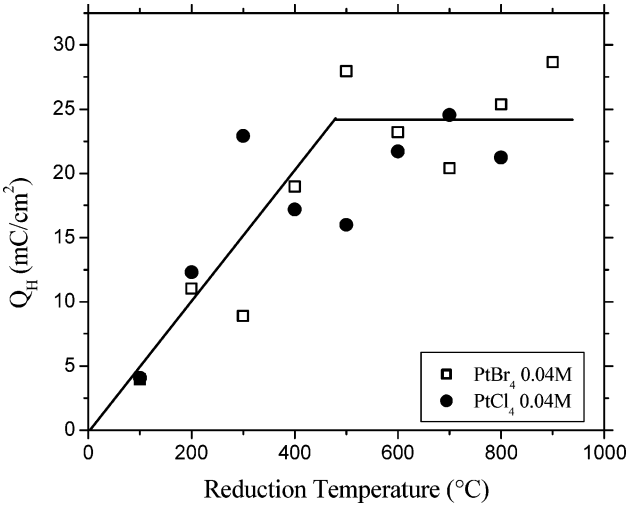

Figure 6. Reduction in H_2/Ar of the Pt precursor adsorbed onto MWCNT grown on fuel cell backing electrodes: effect of the reduction temperature on the value of Q_H measured for these electrodes.

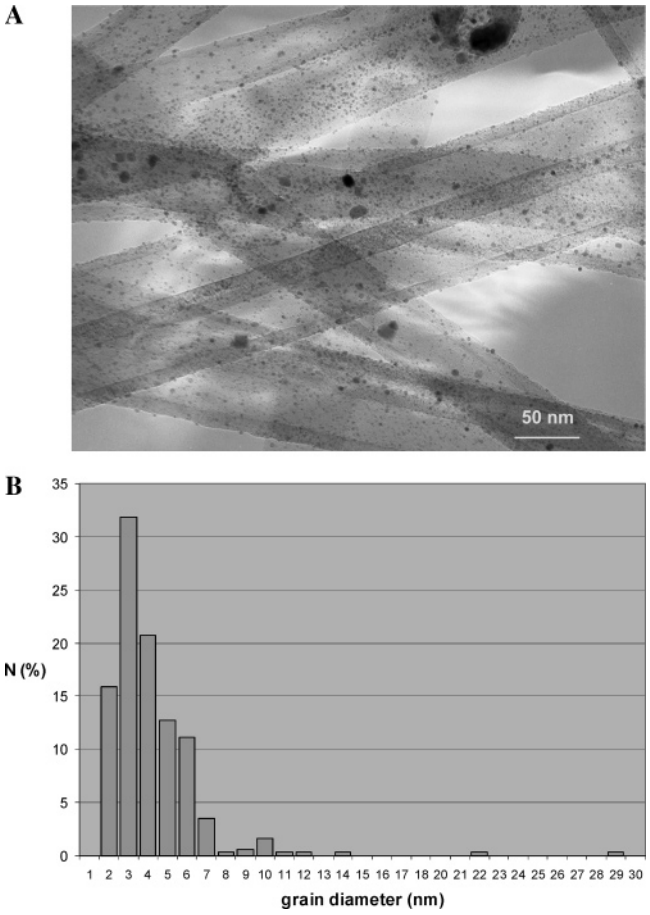

Figure 7. (A) TEM micrograph of a typical Pt−MWCNT−fuel cell backing electrode showing the dispersion of Pt particles of various sizes obtained after chemical reduction in H_2/Ar at 500 °C of the Pt precursor adsorbed on the nanotubes. (B) Histogram of the distribution of Pt particles of Figure 7A.

5B. Most of the Pt (74%) is now detected as Pt(0). However, there is still some Pt(II) (22%) and Pt(IV) (4%) left after the reduction step. The presence of oxidized Pt, especially Pt(II), in the reduced electrode analyzed by XPS is also confirmed by the electronic diffraction of selected areas obtained by TEM. An example of selected area electron diffraction (SAED) is shown in Figure 8. In this figure, the reflections of the (113),

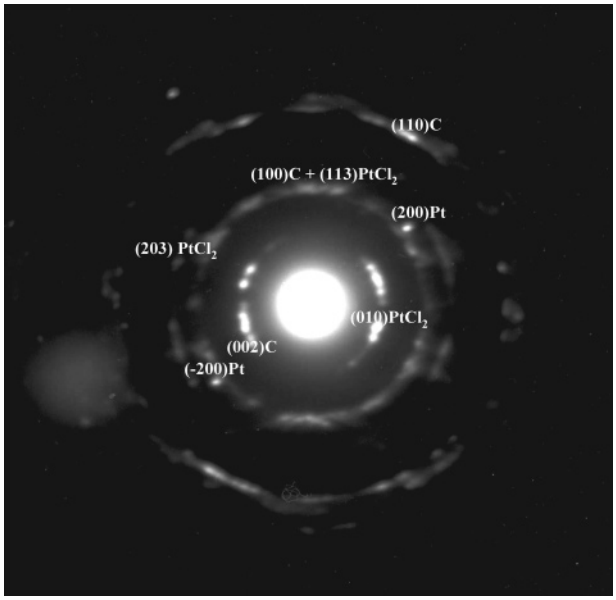

Figure 8. Selected area of electron diffraction (SAED) for the Pt particles obtained after chemical reduction (H_2/Ar) at 500 °C of the Pt precursor deposited from a 0.04 M $PtBr_4$ solution using the silane procedure.

(203), and (010) lattice planes of orthorhombic $PtCl_2$ are also visible as spots on diffraction rings assigned to (100)C and (002)C, while typical (200) spots of metallic Pt appear on the (100) diffraction ring of carbon. $PtCl_2$ is obtained by the reduction of $PtCl_4$, which is the chemical used as the precursor of Pt metal particles. The analyzed region is about 100 nm in size. The incomplete reduction of the Pt precursor on carbon nanotubes has already been mentioned by other authors who also recorded the XPS spectrum of their Pt nanoparticles.[22,28,34]

The results in Figure 6 indicate that after reduction of the adsorbed Pt precursor, the maximum surface active area of Pt (expressed in terms of Q_H) ranges between 20 and 30 mC/cm^2 for a Pt(IV) precursor concentration of 0.04 M. This is much lower than the value of Q_H recorded for Pt-loaded ELAT, for which Q_H values of 70 and 82 mC/cm^2 were measured for 0.35 and 0.40 mg Pt/cm^2. At this point, it therefore becomes important to know the bulk Pt loading of the electrodes made by the silane procedure. This was estimated by neutron activation analysis to be 0.16 mg Pt/cm^2, for the electrodes characterized in Figures 5B, 7, and 8. The value of 0.16 mg Pt/cm^2 is a mean value for three electrodes analyzed. The Pt content of a similar electrode before reduction was 0.15 mg Pt/cm^2. Neutron activation analysis results are accurate within $\pm$ 5%.

Thus, an increase in Pt loading by adsorption of the Pt precursor used in the silane procedure is desired.

One method for increasing Pt loading is by repetitive adsorption from the same solution (0.04 M Pt(IV)) with a reducing step between each adsorption. The Q_H results are shown in Figure 9 (black triangles). Q_H increases linearly with the number of adsorptions to reach more than 60 mC/cm^2 after four adsorptions. Here, each adsorption is followed by a 15 min chemical reduction step in H_2/Ar at 500 °C. Neutron activation analysis reveals that the bulk Pt loading after four successive adsorptions is 0.44 mg Pt/cm^2. This is smaller than $4 \times 0.16 =$ 0.64 mg Pt/cm^2, the expected loading if each adsorption was adding the same Pt content as the first adsorption of Pt onto MWCNTs. The reduction step between each adsorption is necessary. If it is omitted, Q_H only increases to 40 mC/cm^2 and saturates after the third adsorption.

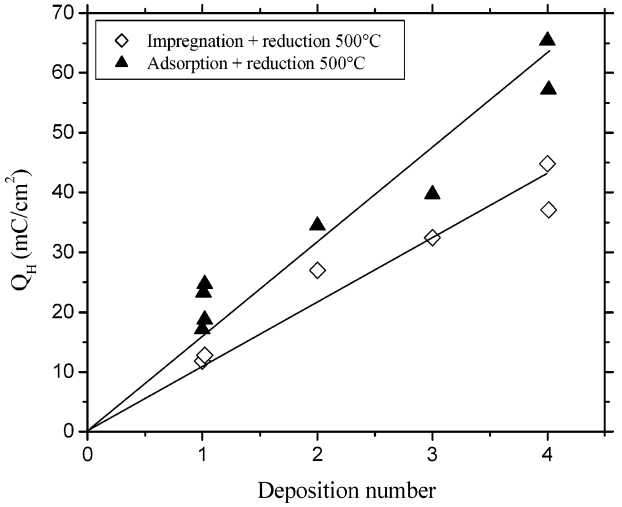

Figure 9. Attempts to increase the active Pt surface area, measured as Q_H, by multiple adsorptions of the Pt precursor (black triangles) or by multiple impregnations from a solution of the Pt precursor (open diamonds).

An alternate method, by impregnation, was also tried to determine if higher Q_H values could be obtained. Here, drops of the Pt precursor silane solution were dropped onto the MWCNT mat and spread homogeneously across the entire electrode as the precursor ethanol solution thoroughly wets the carbon nanotubes. The Q_H values obtained after 4 drop impregnations, each time followed by the reduction of the Pt precursor in H_2/Ar at 500 °C, are also displayed in Figure 9 (open diamonds). The Pt loading after 1 drop is 0.11 mg Pt/cm^2 and reaches 0.40 mg Pt/cm^2 after 4 drops (very close to the 0.44 mg Pt/cm^2 expected). From Figure 9, it may be concluded that the adsorption method for loading Pt onto MWCNTs, for which a higher Q_H value for a lower Pt loading is obtained, leads to better results than the impregnation method. XPS spectra of Pt on MWCNTs were also analyzed for electrodes obtained by impregnation. The Pt4f narrow scan spectrum for an electrode obtained after impregnation of 1 drop and a reduction at 500 °C (not shown) is very similar to that shown in Figure 5B. One may wonder why there is such a difference in the mC/cm^2 and mg Pt/cm^2 readings between one impregnation (a mean value of 13 mC/cm^2 for 0.11 mg Pt/cm^2) and one adsorption (a mean value of 22 mC/cm^2 for 0.16 mg Pt/cm^2) from the same 0.04 M $PtCl_4$ solution. The difference between the two procedures is that a limited volume (1 drop) of solution is spread on 1 cm^2 of electrode (carbon paper + MWCNTs) for the impregnation, while, for adsorption, the same 1 cm^2 of electrode adsorbs a volume of solution larger than 1 drop.

Regarding adsorption of Pt precursor on MWCNTs, another possibility for increasing Q_H would be to *adsorb from more concentrated Pt(IV) precursor solutions*. With this idea in mind, the Pt(IV) salt concentration in the silane solution has been increased from 0.04 to 0.16 M. Doing so, a typical value of Q_H = 47 mC/cm^2 is obtained for a Pt loading of 0.40 mg Pt/cm^2. A TEM micrograph of the Pt particles obtained on MWCNTs using a 0.16 M $PtCl_4$ precursor in solution is shown in the Supporting Information (Figure S2). When it is compared with Figure 7A, it shows that the average Pt particle size did not drastically increase by quadrupling the $PtCl_4$ concentration.

For all the electrodes produced by adsorption or impregnation of the Pt precursor onto the nanotubes, the value of Q_H, obtained after the reduction of the precursor, versus Pt loadings are reported in Figure 10. The Q_H values and Pt loadings of the

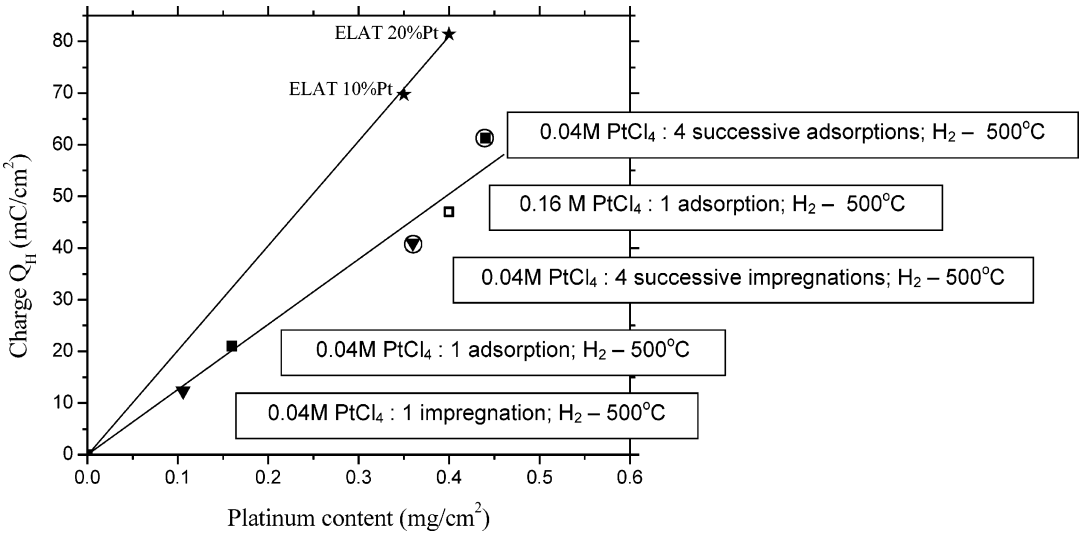

Figure 10. Q_H values vs Pt loadings (after reduction of the Pt precursor) for all the electrodes made by adsorption and impregnation of the Pt precursor onto MWCNTs. Commercial ELAT electrodes are given for comparison.

reference ELAT electrodes are also reported in Figure 10 for comparison. Figure 10 indicates that all electrodes made either by adsorption or impregnation fit a linear trend. This line is less steep than the linear trend for the ELAT references. This implies that, for a similar loading, e.g., 0.4 mg Pt/cm^2, there is more Pt available electrochemically at the surface of the commercial electrode than at the surface of Pt nanoparticles on the carbon nanotubes.

When Q_H values and Pt loadings are known, it is possible to calculate the electrochemically active surface of Pt on carbon nanotubes using the formula detailed in the Experimental Section:

$$S_{EL} = 0.1Q_H/(0.21(\text{Pt loading}))$$

Here, S_{EL} is expressed in m^2/g Pt when Q_H is given in mC/cm^2 and Pt loadings are given in mg Pt/cm^2. A value of $S_{EL} = 63.1$ m^2/g Pt is obtained for 0.04 M $PtCl_4$/1 adsorption H_2–500 °C (Figure 10). The same value is also obtained for all the other loadings of Pt nanoparticles on MWCNTs since all the points belong to the same line. By comparison, $S_{EL} = 97.6$ m^2/g for the two ELAT in Figure 10. A value of 63.1 m^2/g Pt is similar to what is reported for Pt nanoparticles on carbon nanotubes. Typical values found in the literature for S_{EL} are 64.3,[34] 17.2,[32] 95.7[33] 50.4−96.4, depending on the pH during Pt deposition,[24] and 40.6 m^2/g Pt.[48] Values up to 180 m^2/g Pt have been reported in the literature for Pt particles/carbon black.[62]

When the distribution of Pt nanoparticles is also known, it is also possible to calculate the actual surface area of Pt on carbon nanotubes using the formula detailed in the Experimental Section.

$$S_{actual} = 0.1\Sigma(60\,000N_i)/(24.1d_i)$$

Here, S_{actual} is expressed in m^2/g Pt when N_i is the percentage of Pt particles of diameter d_i (in nm) and 24.1 is the Pt density in g/cm^3. A value of $S_{actual} = 81.8$ m^2/g Pt is obtained for 0.04 M $PtCl_4$/1 adsorption H_2−500 °C (Figure 10), using the values for N_i given in the histogram of Figure 7B. Curiously, S_{actual} is larger than S_{EL} and the ratio $100(S_{EL}/S_{actual})$ gives the Pt utilization. Here Pt utilization = (100 × 63.1)/81.8 = 77.1%. A value close to 100% was expected since each Pt nanoparticle is supposed to be in electrical contact with the MWCNT, which is itself in electrical contact with the carbon paper. A possible explanation for this result is that when the electrode contacts the aqueous H_2SO_4 solution, some of the nanotubes form bundles enclosing some of the Pt nanoparticles where access to the aqueous solution is severely restricted. Part of the Pt potentially active surface area is therefore lost in the aggregation process of the nanotubes. The driving force for this aggregation is the hydrophobic character of the nanotubes. This hypothesis is corroborated by the finding that the BET specific surface area of Pt-loaded carbon nanotubes on the carbon paper decreases from 60 to 47 m^2/g after contact of the electrode with the aqueous electrolyte. The ratio of (100 × 47 m^2/g)/(60 m^2/g) = 78% is very close to what was found for Pt utilization (77.1%).

Finally, the Pt loading on MWCNTs has been estimated for Pt/MWCNTs obtained by adsorption of the Pt precursor from a 0.04 and a 0.16 M $PtCl_4$ solution followed by the reduction of the Pt precursor in H_2 at 500 °C. Typical results are 7 and 27 wt % Pt/MWCNTs for 0.04 and 0.16 M $PtCl_4$, respectively. This justifies the choice made of ELAT 10 and 20 wt % Pt/carbon black for comparison.

Pt/MWCNT Used as the Cathode in a Gas Diffusion Electrode Setup. The next step was to use a selected number of the Pt carbon nanotube electrodes for the reduction of oxygen in GDEs. The polarization curves of the selected GDEs are presented (in Tafel representation) in Figure 11A for *iR*-corrected potential versus current delivered by the electrode.

It is obvious from Figure 11A that better polarization curves are obtained with all the electrodes made of Pt on nanotubes as compared with the commercial ELAT electrodes, the best one being the electrode made with 0.16 M $PtCl_4$. This is really surprising since commercial electrodes have a larger Pt area electrochemically available than that of the electrodes bearing Pt on nanotubes. It is speculated that the reason for this improvement is a better diffusion of the H_2SO_4 electrolyte to the catalytic Pt sites located on the carbon nanotubes as compared to the diffusion of the H_2SO_4 electrolyte in ELAT. The Tafel slope calculated from Figure 11A is 58 mV/decade for the commercial electrode. It is difficult to draw a straight line though the experimental points of the electrode bearing the carbon nanotubes because the curves are somewhat concave in the Tafel region. However, if straight lines are drawn through the points between log $I = -3$ and -2 A/cm^2, Tafel slopes of 70, 83, 90, and 96 mV/decade are obtained for CNT + 0.04 M $PtCl_4$ with one adsorption, 0.04 M $PtCl_4$ with two adsorptions,

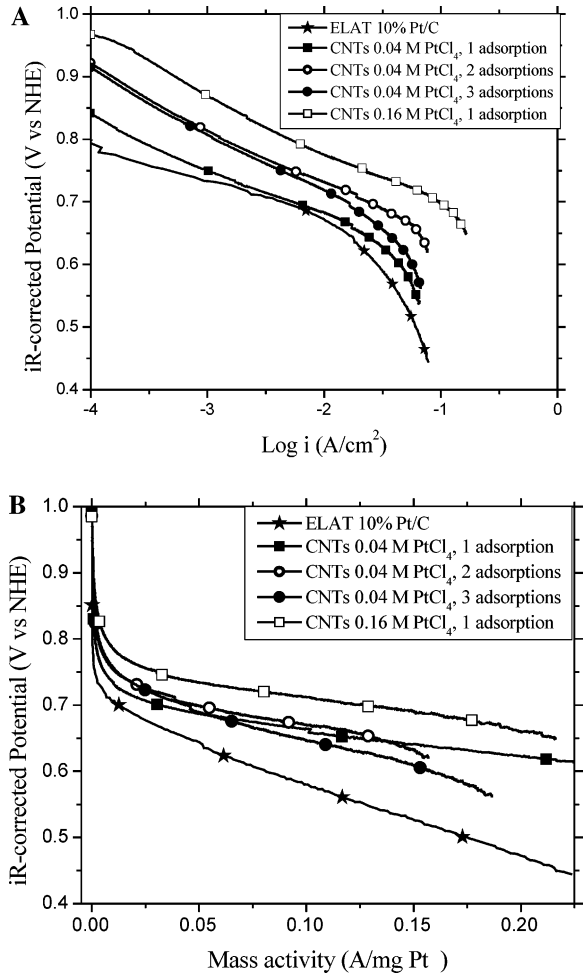

Figure 11. (A) *iR*-corrected polarization curves, in Tafel representation, for the reduction of oxygen in H_2SO_4 at pH 1 for GDEs made of Pt/MWCNTs obtained using the silane procedure and adsorption from various $PtCl_4$ concentrations. A commercial ELAT electrode is given for comparison. (B) Mass activities obtained with the data of part A and Figure 10.

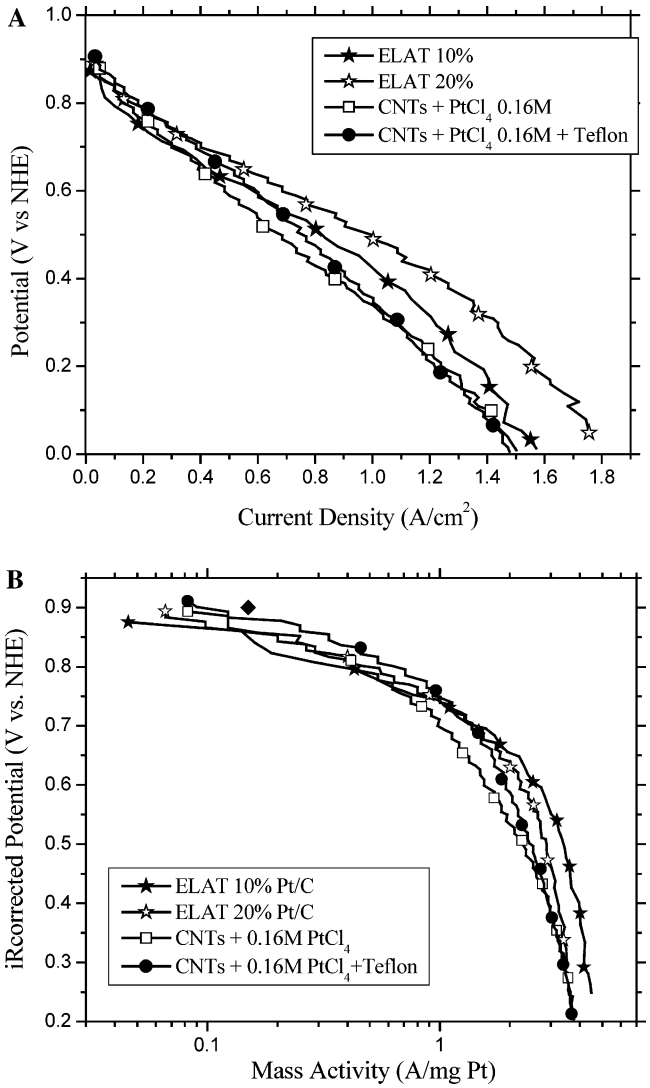

Figure 12. (A) Polarization curves obtained with Pt/MWCNT at the cathode (circles and squares, with or without Teflon at the back of the electrode, respectively). The anode is a 10 wt % Pt/C, 0.35 mg Pt/cm^2 commercial ELAT electrode. The fuel cell was also run with two ELAT electrodes, one at the anode, and the other one at the cathode. (B) Mass activities obtained with the data of part A and Figure 10. Black diamond: reported state-of-the-art activity at 0.9 V for the H_2/saturated O_2 at 65 °C, 100 kPa, for a cathode with 0.4 mg Pt/cm^2 (ref 64).

0.04 M $PtCl_4$ with three adsorptions, and 0.16 M $PtCl_4$ with one adsorption, respectively. Theoretically, a Tafel slope of 60 mV/decade is expected at 25 °C for the reduction of oxygen on Pt electrodes.[63] The higher Tafel slope measured for Pt on nanotubes may be attributed to the very thin insulating silicate layer which is present between the Pt nanoparticles and the carbon collector when Pt nanoparticles are deposited onto the nanotubes using the silane procedure. The fact that all Pt particles which are in contact with the H_2SO_4 electrolyte are also in electrical contact with the collecting electrode for Pt/MWCNTs may be another reason for their better polarization curves compared with those of the commercial electrode.

Figure 11B presents the results of Figure 11A expressed in mass activity. Once again, the mass activities of Pt/MWCNTs are better than the mass activity measured for commercial electrodes. Here, all the curves for the various numbers of adsorptions (from one to three adsorptions from a 0.04 M $PtCl_4$ solution) merge as one polarization curve, while that for the adsorption from a 0.16 M $PtCl_4$ solution remains higher.

Pt/MWCNT Used as the Cathode in Fuel Cell Tests. Finally, we used these Pt/MWCNT electrodes in fuel cell tests with an ELAT electrode with 10 wt % and 20 wt % Pt/C for comparison. Figure 12A shows the polarization curves for the two ELAT electrodes and the electrodes obtained by depositing, by adsorption from a 0.16 M $PtCl_4$ precursor solution, Pt nanoparticles on MWCNTs grown on carbon paper. The best polarization curve for the electrode made with Pt/MWCNTs is obtained by adding a layer of Teflon mixed with carbon black behind the Pt/MWCNT electrode. This polarization curve crosses the best ELAT one at around 0.7 V. Figure 12B presents the polarization curves of Figure 12A (after *iR* correction for the potential), but this time expressed in terms of mass activity. Mass activities for the Pt/MWCNT electrode, slightly higher than that for the ELAT electrode, are also obtained in the same potential region. In order to put these results in perspective, a black diamond has been added on Figure 12B. It represents the state-of-the-art mass activity for 100 kPa saturated O_2 and 65 °C for a cathode having a loading of 0.4 mg Pt/cm^2.[64]

Conclusions

It is possible to grow a large amount of MWCNTs directly on the fibers of commercial porous carbon papers used as carbon-collecting electrodes in fuel cells. It is also possible,

using a silane-based procedure, to deposit Pt nanoparticles on these nanotubes without oxidizing them first. The very thin silicate layer between the Pt particle and the carbon nanotube support, which results from the use of the silane procedure, does not impede the electron transfer between Pt and the collecting electrode. This layer slightly increases, however, the Tafel slope of the ORR, which reaches values up to ~95 mV/decade in H_2SO_4 solution at 25 °C when a value of only 60 mV/decade is expected.

Cyclic voltammetry studies in deaerated H_2SO_4 solution conjugated with TEM and XPS measurements indicate that Pt particles having a median size of 4.1 nm, with a most probable occurrence of 3 nm, are obtained when the Pt precursor is reduced at 500 °C. These particles contain about 75% Pt metal and have an electroactive Pt surface of the order of 60 m^2/g Pt for Pt loadings ranging from 0.1 to 0.45 mg Pt/cm^2. Surprisingly, 60 m^2/g Pt represents only three-fourths of the available Pt surface of all the Pt nanoparticles. The remaining quarter is lost when the nanotubes form bundles in contact with the aqueous H_2SO_4 solution enclosing some of the Pt nanoparticles in the aggregation process. By comparison, a commercial electrode of similar Pt loading (0.35 or 0.40 mg Pt/cm^2) displays a higher electroactive Pt surface area of the order of 100 m^2/g Pt. The Pt loading on MWCNTs is typically 7 wt % when the concentration of the Pt precursor solution is 0.04 M $PtCl_4$ and may reach up to 27 wt % when the concentration of the precursor solution of $PtCl_4$ is increased to 0.16 M.

Although the electroactive Pt surface area is larger for commercial electrodes, the Pt/MWCNT electrode largely outperforms the commercial electrode for the ORR in GDE experiments using H_2SO_4 at pH 1. The better performance of the nanotube electrode is attributed to its 3D character since the nanotubes grow all around each fiber of the 170 μm thick carbon paper, providing an ~200 μm thick active electrode for ORR in contact with the electrolyte. On the other hand, when the same electrodes are used as cathode in H_2/O_2 fuel cell (after having sprayed their back with a mixture of carbon black and Teflon), their polarization curve are only slightly better than the corresponding curves recorded for the commercial electrode at low current densities (in the potential range of ~0.9−0.7 V), while commercial electrodes perform better than Pt/MWCNTs for higher current densities (in the potential range <0.7 V). It is clear that the 3D character of these electrodes is not used in fuel cell conditions since only the Pt nanoparticles, which are very close (within 10 μm) to the membrane, are really active at the cathode (and also at the anode) of H_2/O_2 fuel cells. A large fraction of Pt particles (those which are not within 10 μm of the membrane) will therefore be lost as catalysts for such an electrode architecture. Pt deposited onto loose MWCNTs all spread on the same side of the carbon paper would be a better electrode choice for H_2/O_2 fuel cells. However, it is expected that fuel cells using liquid fuels will be able to fully benefit from the 3D anode electrodes of the type presented in this work.

Acknowledgment. This work is supported by Defense Canada-Valcartier, General Motors of Canada, and NSERC.

Supporting Information Available: A micrograph at lower magnification, depicting MWCNTs covering several fibers and a TEM micrograph of the Pt particles obtained on MWCNTs using a 0.16 M $PtCl_4$ precursor in solution. This material is available free of charge via the Internet at http://pubs.acs.org.

References and Notes

(1) Larminie, J.; Dicks, A. *Fuel Cell Systems Explained*, 2nd ed.; John Wiley & Sons: Chichester, England, 2003.
(2) Gasteiger, H. A.; Kocha, S. S.; Sompalli, B.; Wagner, F. T. *Appl. Catal., B* **2005**, *56*, 9.
(3) Ralph, T. R.; Hogarth, M. P. *Platinum Met. Rev.* **2002**, *46*, 3.
(4) Stamenkovic, V.; Mun, B. S.; Mayrhofer, K. J. J.; Ross, P. N.; Markovic, N. M.; Rossmeisl, J.; Greeley, J.; Norskov, J. K. *Angew. Chem., Int. Ed.* **2006**, *45*, 2897.
(5) Gloaguen, F.; Léger, J. M.; Lamy, C. *J. Appl. Electrochem.* **1997**, *27*, 1052.
(6) Britto, P. J.; Santhanam, K. S. V.; Rubio, A.; Alonso, A.; Ajayan, P. *Adv. Mater.* **1999**, *11*, 154.
(7) Zhang, Y.; Toebes, M. L.; van der Eerden, A.; O'Grady, W. E.; de Jong, K. P.; Koningsberger, D. C. *J. Phys. Chem. B* **2004**, *108*, 18509.
(8) Stonehart, P.; Wheeler, D. *Modern Aspects of Electrochemistry*, No. 38; Conway, B. E., Ed.; Kluwer Academic/Plenum Publishers: New York, 2005; Chapter 4, p 373.
(9) Poncharal, P.; Berger, C.; Yi, Y.; Wang, Z. L.; de Heer, W. A. *J. Phys. Chem. B* **2002**, *106*, 12104.
(10) Cadek, M.; Coleman, J. N.; Ryan, K. P.; Nicolosi, V.; Bister, G.; Fonseca, A.; Nagy, J. B.; Szostak, K.; Béguin, F.; Blau, W. J. *Nano Lett.* **2004**, *4*, 353.
(11) Shao, Y.; Yin, G.; Gao, Y.; Shi, P. *J. Electrochem. Soc.* **2006**, *153*, A1093.
(12) Shao, Y.; Yin, G.; Zhang, J.; Gao, Y. *Electrochim. Acta* **2006**, *51*, 5853.
(13) Li, W.; Wang, X.; Chen, Z.; Waje, M.; Yan, Y. *Langmuir* **2005**, *21*, 9386.
(14) Lee, K.; Zhang, J.; Wang, H.; Wilkinson, D. *J. Appl. Electrochem.* **2006**, *36*, 507.
(15) Chen, W. X.; Lee, J. Y.; Liu, Z. *Mater. Lett.* **2004**, *58*, 3166.
(16) He, Z.; Chen, J.; Liu, D.; Tang, H.; Deng, W.; Kuang, Y. *Mater. Chem. Phys.* **2004**, *85*, 396.
(17) Li, X.; Ge, S.; Hui, C. L.; Hsing, I. M. *Electrochem. Solid−State Lett.* **2004**, *7*, A286.
(18) Girishkumar, G.; Vinodgopal, K.; Kamat, P. V. *J. Phys. Chem. B* **2004**, *108*, 19960.
(19) Xing, Y. *J. Phys. Chem. B* **2004**, *108*, 19255.
(20) Guo, D. J.; Li, H. L. *J. Electroanal. Chem.* **2004**, *573*, 197.
(21) Guo, D. J.; Li, H. L. *Electroanalysis* **2005**, *17*, 869.
(22) Chen, W.; Zhao, J.; Lee, J. Y.; Liu, Z. *Mater. Chem. Phys.* **2005**, *91*, 124.
(23) Huang, J. E.; Guo, D. J.; Yao, Y. G.; Li, H. L. *J. Electroanal. Chem.* **2005**, *577*, 93.
(24) Li, X.; Chen, W. C.; Zhao, J.; Xing, W.; Xu, Z. D. *Carbon* **2005**, *43*, 2168.
(25) Sun, C. L.; Chen, L. C.; Su, M. C.; Hong, L. S.; Chyan, O.; Hsu, C. Y.; Chen, K. H.; Chang, T. F.; Chang, L. *Chem. Mater.* **2005**, *17*, 3749.
(26) Peng, F.; Zhang, L.; Wang, H.; Lv, P.; Yu, H. *Carbon* **2005**, *43*, 2397.
(27) Lin, Y.; Cui, X.; Yen, C.; Wai, C. M. *J. Phys. Chem. B* **2005**, *109*, 14410.
(28) Wu, G.; Chen, Y. S.; Xu, B. Q. *Electrochem. Commun.* **2005**, *7*, 1237.
(29) Mu, Y.; Liang, H.; Hu, J.; Jiang, J.; Wan, L. *J. Phys. Chem. B* **2005**, *109*, 22212.
(30) Qu, L.; Dai, L. *J. Am. Chem. Soc.* **2005**, *127*, 10806.
(31) Kim, Y. T.; Mitani, T. *J. Catal.* **2006**, *238*, 394.
(32) Kongkanand, A.; Kuwubata, S.; Girishkumar, G.; Kamat, P. *Langmuir* **2006**, *22*, 2392.
(33) Zhao, Z. W.; Guo, Z. P.; Ding, J.; Wexler, D.; Ma, Z. F.; Zhang, D. Y.; Liu, H. K. *Electrochem. Commun.* **2006**, *8*, 245.
(34) Tian, Z. Q.; Jiang, S. P.; Liang, Y. M.; Shen, P. K. *J. Phys. Chem. B* **2006**, *110*, 5343.
(35) Ye, J. S.; Cui, H. F.; Wen, Y.; Zhang, W. D.; Guo, Q. X.; Sheu, F. S. *Microchim. Acta* **2006**, *152*, 267.
(36) Qu, L.; Dai, L.; Osawa, E. *J. Am. Chem. Soc.* **2006**, *128*, 5523.
(37) Kim, Y. T.; Ohshima, K.; Higashimine, K.; Uruga, T.; Takata, M.; Suematsu, H.; Mitani, T. *Angew. Chem., Int. Ed.* **2006**, *45*, 407.
(38) Wang, H. J.; Yu, H.; Peng, F.; Lv, P. *Electrochem. Commun.* **2006**, *8*, 499.
(39) Liu, Z.; Lin, X.; Lee, J. Y.; Zhang, W.; Han, M.; Gan, L. M. *Langmuir* **2002**, *18*, 4054.
(40) Li, W.; Liang, C.; Qiu, J.; Zhou, W.; Han, H.; Wei, Z.; Sun, G.; Xin, Q. *Carbon* **2002**, *40*, 787.
(41) Li, W.; Liang, C.; Zhou, W.; Qiu, J.; Zhou, Z.; Sun, G.; Xin, Q. *J. Phys. Chem. B* **2003**, *107*, 6292.
(42) Matsumoto, T.; Komatsu, T.; Nakano, H.; Arai, K.; Nagashima, Y.; Yoo, E.; Yamazaki, T.; Kijima, M.; Shimizu, H.; Takasawa, Y.; Nakamura, J. *Catal. Today* **2004**, *90*, 277.

(43) Li, W.; Liang, C.; Zhou, W.; Qiu, J.; Li, H.; Sun, G.; Xin, Q. *Carbon* **2004**, *42*, 423.
(44) Wang, C.; Waje, M.; Wang, X.; Tang, J. M.; Haddon, R. C.; Yan, Y. *Nano Lett.* **2004**, *4*, 345.
(45) Matsumoto, T.; Komatsu, T.; Arai, K.; Yamazaki, T.; Kijima, M.; Shimizu, H.; Takasawa, Y.; Nakamura, J. *Chem. Commun.* **2004**, 840.
(46) Yuan, F.; Ryu, H. *Nanotechnology* **2004**, *15*, S596.
(47) Rajalakshmi, N.; Ryu, H.; Shaijumon, M. M.; Ramaprabhu, S. *J. Power Sources* **2005**, *140*, 250.
(48) Wang, X.; Waje, M.; Yan, Y. *Electrochem. Solid—State Lett.* **2005**, *8*, A42.
(49) Liu, Z.; Gan, L. M.; Hong, L.; Chen, W.; Lee, J. Y. *J. Power Sources* **2005**, *139*, 73.
(50) Waje, M.; Wang, X.; Li, W.; Yan, Y. *Nanotechnology* **2005**, *16*, S395.
(51) Xu, C.; Chen, J.; Cui, Y.; Han, Q.; Choo, H.; Liaw, P. K.; Wu, D. *Adv. Eng. Mater.* **2006**, *8*, 73.
(52) Shao, Y.; Yin, G.; Wang, J.; Gao, Y.; Shi, P. *J. Power Sources* **2006**, *161*, 47.
(53) Dujardin, E.; Ebessen, T. W.; Hiura, H.; Tanigaki, K. *Science* **1994**, *265*, 1850.
(54) Hwang, K. C. *J. Chem. Soc., Chem. Commun.* **1995**, 173.
(55) Lago, R. M.; Tsang, S. C.; Lu, K. L.; Chen, Y. K.; Green, M. L. H. *J. Chem. Soc., Chem. Commun.* **1995**, 1355.
(56) Tsang, S. C.; Chen, Y. K.; Harris, P. J. F.; Green, M. L. H. *Nature* **1994**, *372*, 159.
(57) Sun, X.; Li, R.; Villers, D.; Dodelet, J. P.; Désilets, S. *Chem. Phys. Lett.* **2003**, *379*, 99.
(58) Sun, X.; Stansfield, B.; Dodelet, J. P.; Désilets, S. *Chem. Phys. Lett*. **2002**, *363*, 415.
(59) Sun, X.; Li, R.; Lebrun, G.; Stansfield, B.; Dodelet, J. P.; Désilets, S. *Int. J. Nanosci.* **2002**, *1*, 223.
(60) Lalande, G.; Denis, M. C.; Guay, G.; Dodelet, J. P.; Schulz, R. *J. Alloys Compd.* **1999**, *292*, 301.
(61) Woods, R. *J. Electrochem. Soc.* **1976**, *9*, 1.
(62) Stonehart, P. *Ber. Bunsen-Ges Phys. Chem.* **1990**, *94*, 913.
(63) Sepa, D. B.; Vojnovic, M. V.; Vracar, L. M. *Electrochim. Acta* **1984**, *29*, 1169.
(64) Kocha, S. S. *Handbook of Fuel cells—Fundamentals, Technology and Applications*; Vielstich, W., Gasteiger, H., Lamm, A., Eds.; John Wiley & Sons: New York, 2003; Chapter 43.